J. DIFERENSIAL/E-ISSN:2775-9644
Vol.6(2),2024, 108–123
doi:https://doi.org/10.35508/jd.v6i2.13188

RESEARCH ARTICLE

Coupled Effects of Magnetohydrodynamics and Nanoparticles on Nonlinear Stretching Wedge Flow with Multiple Slips and Non-Uniform Heating

Victor Adetayo Akinrinmade[1,*], Mutairu Kayode Kolawole[2]

[1]*Department of Mathematics and Statistics, Osun State College of Technology, Esa-Oke, Osun State, Nigeria*
[2]*Department of Mathematical Sciences, Osun State University, Osogbo, Nigeria*
[*]*Corresponding author: akinrinmadevictor@gmail.com*

Received: 7 November 2023; Revised: 26 April 2024; Accepted: 9 May 2024; Published:4 June 2024.

Abstract:
This study investigates the complex interplay between magnetohydrodynamics (MHD), nanoparticle behavior, and fluid flow characteristics in the context of a nonlinear stretching wedge with multiple slips and non-uniform heating. The flow is driven by a water-based fluid containing nano-sized particles of aluminum oxide and copper $(Al_2O_3 - Cu/H_2O)$. The governing equations of the problem are derived and then solved using appropriate numerical techniques. The effects of various parameters such as the magnetic field strength, nanoparticle volume fraction, wedge angle, slip parameters, and non-uniform heat source are thoroughly analyzed. Results reveal significant alterations in the flow behavior due to the presence of nanoparticles and the applied magnetic field. The interaction between the fluid flow and magnetic field induces a substantial change in velocity and temperature distributions along the wedge surface. Moreover, the slip effects and non-uniform heat source further modify the flow characteristics. This investigation provides valuable insights into the coupled effects of MHD, nanoparticles, and slip conditions on the flow dynamics and thermal behavior in nonlinear stretching wedge configurations. Such insights are crucial for understanding and optimizing processes involving fluid flow and heat transfer in engineering applications, particularly those utilizing nano-fluids and magnetic fields.

Keywords: Magnetohydrodynamics (MHD), Nanoparticles, Nonlinear stretching wedge, multiple slips, Non-uniform heating

1. Introduction

In recent years, the exploration of magnetohydrodynamics (MHD) coupled with nanoparticle-laden fluids has garnered significant attention due to its wide-ranging implications in various engineering and industrial applications. This burgeoning field encompasses the study of fluid flow behavior in the presence of both magnetic fields and nanoparticles, offering a unique avenue for enhancing heat transfer and fluid transport processes. Among the numerous configurations studied in MHD literature, nonlinear stretching wedges stand out as versatile geometries with applications in boundary

layer control, aerodynamics, and materials processing in [1–3]. The inherent complexity of fluid flow in these geometries, compounded by the introduction of nanoparticles and non-uniform heat sources, underscores the need for comprehensive investigations to elucidate the underlying phenomena and optimize performance. This encapsulates the key focal points of this research endeavor [4]. This study aims to delve into the intricate interactions between MHD, nanoparticle dynamics, slip conditions, and non-uniform heating in the context of fluid flow over a nonlinear stretching wedge. By dissecting and analyzing these coupled effects, the research endeavors to advance our understanding of complex fluid dynamics and thermal behavior in practical engineering scenarios by [5, 6]. The utilization of nanoparticle-laden fluids introduces novel challenges and opportunities in fluid dynamics and heat transfer. Nanoparticles, due to their minuscule size and large surface area-to-volume ratio, exhibit unique properties that can significantly influence fluid behavior and thermal characteristics. In this study, the nanoparticles under consideration consist of aluminum oxide and copper suspended in a water-based fluid [7]. The choice of nanoparticles is motivated by their widespread availability, thermal conductivity, and potential applications in thermal management systems and nanofluidic devices [8]. The presence of a magnetic field further complicates the fluid dynamics, as MHD effects arise from the interaction between the magnetic field and the electrically conducting fluid. This interaction induces Lorentz forces that alter the fluid flow patterns and heat transfer rates. Understanding the interplay between MHD and nanoparticle dynamics is crucial for optimizing processes such as magnetofluidic pumping, magnetic drug targeting, and magnetic hyperthermia treatments. The nonlinear stretching wedge geometry serves as a pertinent model for investigating boundary layer flow phenomena and fluid-solid interactions [9]. As the wedge stretches or contracts nonlinearly, it induces variations in velocity and temperature gradients along its surface, leading to complex flow patterns and heat transfer characteristics. By studying fluid flow over such geometries, researchers can glean insights into boundary layer development, separation control, and drag reduction techniques. [10] To the geometric complexity, the inclusion of multiple slip conditions introduces further intricacies into the flow dynamics. Slip boundary conditions, characterized by the relative motion between the fluid and solid surfaces, play a pivotal role in determining the flow behavior near the boundary. Understanding the influence of slip conditions on fluid transport and heat transfer is imperative for optimizing the performance of microfluidic devices, lubrication systems, and surface coating processes [11, 12]. The imposition of a non-uniform heat source adds another layer of complexity to the problem. Non-uniform heating profiles, arising from practical considerations or external factors, can significantly alter temperature distributions and thermal gradients within the fluid domain. Investigating the combined effects of non-uniform heating, MHD, nanoparticle dynamics, and slip conditions provides valuable insights into thermal management strategies, energy conversion systems, and heat exchanger design [13]. To unravel the intricate interplay between magnetohydrodynamics, nanoparticles, slip conditions, and non-uniform heating in the context of fluid flow over a nonlinear stretching wedge. By comprehensively analyzing these coupled effects, the study seeks to advance our understanding of complex fluid dynamics and thermal behavior, thereby facilitating the development of innovative solutions for engineering challenges in various domains. The exploration of coupled effects in magnetohydrodynamics (MHD) and nanoparticle-laden fluids represents a frontier in interdisciplinary research, bridging the realms of fluid mechanics, electromagnetism, and nanotechnology [14–16]. The integration of MHD principles with nanoparticle dynamics offers a promising avenue for enhancing heat transfer rates, improving fluid transport efficiency, and designing novel functional materials with tailored properties. The synergistic effects arising from the interaction between magnetic fields and nanoparticles have been harnessed in diverse fields ranging from biomedical engineering to aerospace propulsion. In biomedical applications, MHD-driven nanoparticle transport holds promise for targeted drug delivery, where magnetic nanoparticles serve as carriers for therapeutic agents, guided and localized within the body via external magnetic fields [17]. Additionally, magnetic hyperthermia treatments leverage the ability of magnetic nanoparti-

cles to generate heat under alternating magnetic fields, selectively ablating cancerous tissues while minimizing damage to healthy cells. The precise control afforded by MHD techniques offers a versatile platform for advancing the efficacy and safety of therapeutic interventions. Energy conversion and storage, MHD-based systems offer potential solutions for improving the efficiency of power generation and heat transfer processes. Magnetohydrodynamic generators harness the kinetic energy of conductive fluids in the presence of magnetic fields to produce electrical power, offering an alternative approach to traditional turbine-based generators [18]. Furthermore, the integration of nanoparticles into heat transfer fluids enhances thermal conductivity and convective heat transfer coefficients, leading to more efficient heat exchangers, solar collectors, and thermal energy storage systems. In aerospace and propulsion engineering, the application of MHD principles in conjunction with nanoparticle-laden fluids holds promise for advancing propulsion technologies and aerodynamic control systems [19–22]. Magnetohydrodynamic propulsion systems, utilizing ionized gases or conductive fluids accelerated by magnetic fields, offer potential solutions for achieving high-speed propulsion with reduced fuel consumption and emissions. Additionally, the manipulation of fluid flow characteristics using MHD techniques enables precise control of aerodynamic forces, leading to enhanced maneuverability and efficiency in aerospace vehicles [23]. Overall, the integration of magnetohydrodynamics and nanoparticles represents a paradigm shift in the design and optimization of engineering systems, offering unprecedented opportunities for innovation and advancement across diverse fields [24–26]. Through comprehensive investigations into the coupled effects of MHD, nanoparticles, slip conditions, and non-uniform heating, this research endeavor seeks to contribute to the foundational knowledge and practical applications of this emerging interdisciplinary field.

2. Materials and Methods

We assume a Falkner–Skan flow of an incompressible unsteady tangent hyperbolicnanofluid over a faster/slower stretching wedge in light of an applied magnetic field along with activation energy and magnetic field. The Reynolds number is considered very small, and prompted magnetic field would ignore. The fluid is assumed to be Newtonian, electrically conducting and its property variations due to temperature and induced magnetic field are limited to fluid density.
Also, the induced magnetic field is assumed to be either also contribute to the fluid flow properties. Let the $x-$axis be taken along the direction of plate and $y-$axis normal to it. If u,v,T and B_i,$i = 1, 2$ are the fluid x-component of velocity, $y-$component of velocity, temperature and induced magnectic respectively. Further, we considered that fluid flow is caused by stretching wedge with the velocity

$$u_w(x,t) = \frac{bx^m}{1-ct} \tag{2.1}$$

The free stream velocity for the current problem is

$$u_e(x,t) = \frac{ax^m}{1-ct} \tag{2.2}$$

where m, a, b, c are positive constants with $0 \leq m \leq 1$, and $ct < 1$. The angle of the wedge is supposed to be

$$\Omega = \pi\beta, \text{ where } \beta = \frac{2m}{1+m} \tag{2.3}$$

symbolizes the wedge angle parameter. From the perspective of White, positive value of $\beta(\beta > 0)$ provides acceleration to the fluid flow and negative value of $\beta(\beta < 0)$ generates retardation. Additionally, $\beta = 0$ (i.e.,$m = 0$) corresponds to boundary layer flow over a horizontal flat plate and $\beta = 1$ (i.e.,$m = 1$) relate to boundary layer flow near the stagnation point of a vertical flat plate. Further, we assume that (concentrations, temperature) at the wedge surface (C_w, T_w) are higher than

the ambient (concentrations, temperature) i.e., (C_∞, T_∞) that is , $C_w > C_\infty$, and $T_w > T_\infty$. The Cartesian coordinates (x, y) is utilized with x correspond coincides with the surface of the wedge and y perpendicular to it, and $y \leq 0$ is the fluid occupied region (see Figure 2). Also, the fluid binary reaction under the influence of moving flat surface, buoyance forces and magnetic field occurs in a permeable device with isothermal boundary layer. The chemical mixture for a single exothermic reaction with continuous particle collision is propelled by chemical heat generation and chemical kinetics.

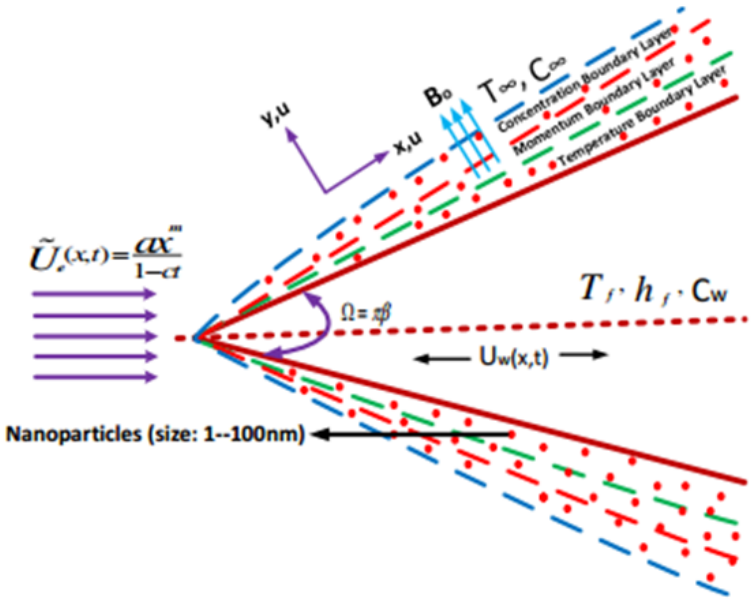

Figure 2.1: Schematic flow of distribution.

3. Model Analysis

The combined velocity of the stretching sheet and the slip condition was provided by $u = u_w(x,t) + vL\frac{\partial u}{\partial y}$, whereas $u \to u_e(x,t)$ provide the velocity of stagnation point. Moreover,$v_w, -k\frac{\partial T}{\partial y} = h(Tw\breve{}T)$ and B
Respectively sets out the suction velocity, convective heat transfer, and the magnetic flux provided at acute angle

$$\Phi = \frac{\pi}{2}\, rad \tag{3.4}$$

$$\frac{\partial u}{\partial x} + \frac{\partial u}{\partial y} = 0 \tag{3.5}$$

$$\frac{\partial B_1}{\partial x} + \frac{\partial B_2}{\partial y} = 0 \tag{3.6}$$

Momentum Equation

$$\begin{aligned} &\frac{\partial u}{\partial t} + u\frac{\partial u}{\partial x} + v\frac{\partial u}{\partial y} = u_\ell \frac{\partial u_\ell}{\partial x} - \left[\frac{\mu_{nf}}{\rho_{nf}}\left(1+\frac{1}{\gamma}\right) + \sqrt{2nf}\left(\frac{\partial u}{\partial y}\right)\right]\frac{\partial^2 u}{\partial y^2} \pm \frac{g}{\rho_{nf}}\left(\frac{k_1}{v}\right)|\hat{u}| \\ &(u-U) - \frac{\mu_\ell}{4\pi\rho_{nf}}\left(B_1\frac{\partial B_1}{\partial x} + B_2\frac{\partial B_1}{\partial y} - B_0\frac{dB_0}{dx} + \frac{g}{\rho_{nf}}\left[\beta\tau\left(T-T_\infty\right) + B_c\left(C-C_\infty\right)\right]\right) \end{aligned} \tag{3.7}$$

Induced Magnetic Field Equation

$$\frac{\partial B_1}{\partial t}+u\frac{\partial B_1}{\partial x}+v\frac{\partial B_1}{\partial y}=B_1\frac{\partial u}{\partial x}+B_2\frac{\partial u}{\partial y}+\mu_0\frac{\partial^2 B_1}{\partial y^2}-\frac{k_{nf}}{(\rho c)_{nf}}\frac{\partial q_r}{\partial y^r} \tag{3.8}$$

Energy Transfer Equation

$$\begin{aligned}\frac{\partial T}{\partial t}+u\frac{\partial T}{\partial x}+v\frac{\partial T}{\partial y}&=\frac{k_{hnf}}{(\rho c_p)_{hnf}}\frac{\partial^2 T}{\partial y^2}\\ +N_{nf}\left[D_m\frac{\partial T}{\partial y}\frac{\partial C}{\partial y}+\frac{D_t}{T_\infty\left(\frac{\partial T}{\partial y}\right)^2}+\left(1+\frac{1}{\gamma}\right)\left(\frac{\partial u}{\partial y}\right)^2\right]&\\ +\frac{1}{\sigma\left(c_p\rho\right)_{nf}}\left(\frac{\partial B_1}{\partial y}\right)^2+\frac{q'''}{(\rho c_p)_{hnf}}&\end{aligned} \tag{3.9}$$

Mass transfer (species) equation becomes

$$\frac{\partial C}{\partial t}+u\frac{\partial C}{\partial x}+v\frac{\partial C}{\partial y}=\frac{\partial C_m}{\rho_{nf}}\frac{\partial^2 C}{\partial y^2}+\frac{D_T}{\rho_{nf}T_\infty}\frac{\partial^2 T}{\partial y^2}-\frac{k'^m v}{\tau\rho_{nf}}\frac{\partial}{\partial y}\left[\left(C-C_\infty\right)V_T\right] \tag{3.10}$$

$$\begin{aligned}\frac{\partial C}{\partial t}+u\frac{\partial T}{\partial x}+v\frac{\partial T}{\partial y}&=\frac{k_{nf}}{(\rho C_p)_{nf}}\frac{\partial^2 T}{\partial y^2}+\frac{\mu_{nf}}{(\rho C_p)_{nf}}\left(1+\frac{1}{\gamma}\right)\left(\frac{\partial u}{\partial y}\right)^2\\ +\frac{\mu_0}{\sigma\left(\rho C_p\right)_{nf}}\left(\frac{\partial B_1}{\partial y}\right)^2+\frac{\tau}{\rho_{nf}}\left(D_m\frac{\partial C}{\partial y}+\frac{D_T}{T_\infty}\frac{\partial T}{\partial y}\right)\frac{\partial T}{\partial y}+\frac{\sigma}{(\rho C_p)_f}B^2u^2&\\ +\frac{k_{nf}}{(\rho C_p)_{nf}}\frac{16\sigma T_\infty^3}{3k_s}\frac{\partial^2 T}{\partial y^2}+\frac{ku_w\left(x\right)}{x\left(\rho C_p\right)_{nf}}\left[\frac{\dot{A}\left(T_w-T_\infty\right)}{bx}u+\dot{B}\left(T-T_\infty\right)\right]&\end{aligned}$$

$$\begin{aligned}\frac{\partial C}{\partial t}+u\frac{\partial C}{\partial x}+v\frac{\partial C}{\partial y}&=\frac{D_m}{\rho_{nf}}\frac{\partial^2 C}{\partial y^2}+\frac{D_T}{\rho_{nf}T_\infty}\frac{\partial^2 T}{\partial y^2}-\frac{k'\mu_{nf}}{\Xi\rho_{nf}}\frac{\partial}{\partial y}\\ \left(C-C_\infty\right)\frac{\partial T}{\partial y}-k_r^2\left(\frac{T}{T_\infty}\right)^r exp\left(-\frac{E_a}{R_GT}\right)\left(C-C_\infty\right)&\end{aligned} \tag{3.11}$$

$$\frac{\partial C}{\partial t}+u\frac{\partial C}{\partial x}+v\frac{\partial C}{\partial y}=\frac{D_m}{\rho_{nf}}\frac{\partial^2 C}{\partial y^2}+\frac{D_T}{\rho_{nf}T_\infty}\frac{\partial^2 T}{\partial y^2}-\frac{k'\mu_{nf}}{\Xi\rho_{nf}}\frac{\partial}{\partial y}\left(C-C_\infty\right)\frac{\partial T}{\partial y} \tag{3.12}$$

The boundary conditions at the plate surface and far into the cold fluid may be written as:

$$\begin{aligned}t<0:\quad & u_w\left(x\right),\ v=0,\ \tfrac{\partial B_1}{\partial y}=B_2=0,\ T=T_w,\ C=C_w,\ \forall\, y\\ t\geq 0:\ &\left\{\begin{array}{c}u_w\left(x\right)+N\left(1+\frac{1}{\gamma}\right)\frac{\partial u}{\partial y},\ v=0,\ \frac{\partial B_1}{\partial y}=B_2=0\\ -k_{nf}\frac{\partial T}{\partial y}=h\left(T_w-T\right),\ D_B\frac{\partial C}{\partial y}+\frac{D_T}{T_\infty}\frac{\partial T}{\partial y}=0\end{array}\right\},\ \text{at } y=0\\ &u\to U_\infty,\ B_1\to B_e,\ T\to T_\infty,\ C\to C_\infty,\quad \text{as } y\to\infty\end{aligned} \tag{3.13}$$

where his the plate heat transfer coefficient,T_w is the plate temperature of the hot fluid at the left surface of the plate and k_{hnf} is the thermal conductivity coefficient. D_B and D_T are the Brownian diffusion and thermophoretic diffusion coefficient respectively, u_e is the free stream velocity,

$B_0, m, \rho, c_p, E_a, n$ and Γ are the uniform magnetic field strength, Falkner–Skan power law parameter, fluid density, specific heat capacity, activation energy, the power law index, and Williamson parameter, respectively.
Under the above assumptions, the system of equations governing the flow because, the system is reduced to

$$\begin{aligned}
\frac{\partial u}{\partial x}+\frac{\partial v}{\partial y}&=0\\
\frac{\partial B_1}{\partial x}+\frac{\partial B_2}{\partial y}&=0\\
\frac{\partial u}{\partial x}+v\frac{\partial u}{\partial y}=\frac{\partial u_e}{\partial t}+(1-n)\frac{\mu_{nf}}{\rho_{nf}}\frac{\partial^2 u}{\partial y^2}+\sqrt{2}n\Gamma\frac{\mu_{nf}}{\rho_{nf}}\left(\frac{\partial u}{\partial y}\right)\frac{\partial^2 u}{\partial y^2}&\\
-\frac{\sigma B_1^2(t)}{\rho}(u-u_e)+\frac{\mu_e}{4\pi\rho_{nf}}\left(B_1\frac{\partial B_1}{\partial x}+B_2\frac{\partial B_1}{\partial y}-B_e\frac{dB_e}{dx}\right)&\\
+u_e\frac{du_e}{dx}+\frac{g\beta}{\rho_{nf}}(T-T_\infty)+\frac{g\beta_C}{\rho_{nf}}(C-C_\infty)&\\
u\frac{\partial B_1}{\partial x}+v\frac{\partial B_1}{\partial y}=B_1\frac{\partial u}{\partial x}+B_2\frac{\partial u}{\partial y}+\mu_0\frac{\partial^2 B_1}{\partial y^2}&
\end{aligned}\tag{3.14}$$

$$\begin{aligned}
u\frac{\partial T}{\partial x}+v\frac{\partial T}{\partial y}=\frac{k_{nf}}{(\rho c_p)_{nf}}\frac{\partial^2 T}{\partial y^2}+\frac{\mu_{nf}}{(c_p\rho)_{nf}}\left(1+\frac{1}{\gamma}\right)\left(\frac{\partial u}{\partial y}\right)^2&\\
+\frac{\mu_0}{\sigma(c_p\rho)_{nf}}\left(\frac{\partial B_1}{\partial y}\right)^2+\frac{\tau}{\rho_{n_f}}\left(D_m\frac{\partial C}{\partial y}+\frac{D_T}{T_\infty}\frac{\partial T}{\partial y}\right)\frac{\partial T}{\partial y}+\frac{\sigma}{(\rho c)_f}B_0^2u^2&\\
+\frac{k_{nf}}{(\rho c_p)_{nf}}\frac{16\sigma T_\infty^3}{3k_s}\frac{\partial^2 T}{\partial y^2}+\frac{\kappa u_w(x)}{x(\rho c_p)_{nf}}\left[\frac{A^*(T_w-T_\infty)}{bx}u+B^*(T-T_\infty)\right]&
\end{aligned}\tag{3.15}$$

$$\begin{aligned}
&x=0:\quad u_w(x),\ v=0,\ \tfrac{\partial B_1}{\partial y}=B_2=0,\ T=T_w,\ C=C_w,\ \forall\, y\\
&x\geq 0,\left\{\begin{array}{c} u_w(x)+N\left(1+\frac{1}{\gamma}\right)\frac{\partial u}{\partial y},\ v=0,\ \frac{\partial B_1}{\partial y}=B_2=0\\ -k_{nf}\frac{\partial T}{\partial y}=h(T_w-T),\end{array}\right\},\ \text{at } y=0\\
&\qquad\qquad u\to U_\infty,\ B_1\to B_e,\ T\to T_\infty,\quad \text{as } y\to\infty
\end{aligned}\tag{3.16}$$

where

$$N_f(f,\ g,\ \theta)$$

$$N_g(f,\ g,\ \theta)=\frac{\partial^3 g(\eta)}{\partial\eta^3}+\frac{A_5}{Pm}\left(f(\eta)\frac{\partial^2 g(\eta)}{\partial\eta^2}-g(\eta)\frac{\partial^2 f(\eta)}{\partial\eta^2}\right)-\frac{\alpha_1}{2}\left(\frac{\partial g(\eta)}{\partial\eta}+\eta\frac{\partial^2 g(\eta)}{\partial\eta^2}\right)=0$$

For

$$\begin{aligned}
f'(\eta,0)=1+V\left(1+\frac{1}{\gamma}\right)\frac{\partial^2 f(\eta,0)}{\partial\eta^2}, f(\eta,0)=S, g''(\eta,0)=0, g(\eta,0)=0,&\\
Bi\frac{\partial\theta(\eta,0)}{\partial\eta}=-(1-\theta(\eta,0)), \omega\frac{\partial\phi(\eta,0)}{\partial\eta}=-(1-r\theta(\eta,0)&
\end{aligned}\tag{3.17}$$

and for $p=1$,

$$\frac{\partial f(\eta,1)}{\partial\eta}=\lambda,\ \frac{\partial g(\eta,\ 1)}{\partial\eta}=1, \theta(\eta,\ 1)=0,\ \phi(\eta,\ 1)=0\tag{3.18}$$

As p changes from 0 to 1, $f_0(\eta)$, $g_0(\eta)$ and $\theta_0(\eta)$ approach $f(\eta,\ p)$, $g(\eta,\ p)$ and $\theta(\eta,\ p)$ respectively.
By Taylor's series expansion,

$$f(\eta;\ p)\ =\ f_0(0)+\sum_{n=1}^{\infty}f_m(\eta)\,p^n\tag{3.19}$$

$$g(\eta;\ p) \ = \ g_0(0) + \sum_{n=1}^{\infty} g_m(\eta)\, p^n$$

$$\theta(\eta;\ p) \ = \ \theta_0(0) + \sum_{n=1}^{\infty} \theta_m(\eta)\, p^n$$

$$\phi(\eta;\ p) \ = \ \phi_0(0) + \sum_{n=1}^{\infty} \phi_m(\eta)\, p^n \tag{3.20}$$

where

$$f_m(\eta;\ p) = \frac{1}{k!}\frac{\partial^m}{\partial \eta^m} f(\eta;\ p) \tag{3.21}$$

$$g_m(\eta;\ p) = \frac{1}{k!}\frac{\partial^m}{\partial \eta^m} g(\eta;\ p) \tag{3.22}$$

$$\theta_m(\eta;\ p) = \frac{1}{k!}\frac{\partial^m}{\partial \eta^m} \theta(\eta;\ p) \tag{3.23}$$

$$\phi_m(\eta;\ p) = \frac{1}{k!}\frac{\partial^m}{\partial \eta^m} \phi(\eta;\ p) \tag{3.24}$$

At $p = 1$ the series equations 1 and 2 converge if the following parameters: initial guesses, auxiliary linear operators, and the auxiliary are chosen appropriately. Hence,

$$f(\eta) \ = \ f_0(\eta) + \sum_{n=1}^{\infty} f_m(\eta) \tag{3.25}$$

$$g(\eta) \ = \ g_0(\eta) + \sum_{n=1}^{\infty} g_m(\eta) \tag{3.26}$$

$$\theta(\eta) \ = theta_0(\eta) + \sum_{n=1}^{\infty} \theta_m(\eta) \tag{3.27}$$

$$\phi(\eta) \ = \ \phi_0(\eta) + \sum_{n=1}^{\infty} \phi_m(\eta) \tag{3.28}$$

The *dth-order* deformation problems are:

$$L_f(f_d - \ \chi_d f_{d-1} \ = \ \hbar_f R_d^f(\eta) \tag{3.29}$$

$$L_g(g_d - \chi_d g_{d-1} \ = \ \hbar_g R_d^g(\eta) \tag{3.30}$$

$$L_\theta(\theta_d - \chi_d \theta_{d-1} \ = \ \hbar_\theta R_d^\theta(\eta) \tag{3.31}$$

$$L_\Phi(\Phi_d - \chi_d \Phi_{d-1} \ = \ \hbar_\theta R_d^\Phi(\eta) \tag{3.32}$$

With the conditions:

$$f_d'(\eta, 0) = 1 + V\left(1 + \frac{1}{\gamma}\right) f_d''(0), f_d(\eta) = S,\ f_d'(\infty) = \lambda, \tag{3.33}$$

$$g_d''(\eta) = 0, g_d(\eta) = 1,\ g_d'(\infty) \tag{3.34}$$

$$Bi\frac{\partial\theta_d(\eta)}{\partial\eta,} = -\left(1-\theta_d(\eta)\right), \theta_d(\infty) = 0, \tag{3.35}$$

$$\omega\frac{\partial\phi_d(\eta,0)}{\partial\eta,} = -\left(1-r\theta_d(\eta,0)\right), \ \phi_d(\infty) = 0 \tag{3.36}$$

Where

$$\begin{aligned} R_d^f(\eta) \ = & \left(\left(1+\frac{1}{\gamma}\right)+\delta\sum_{k=1}^{d=1} f''_{d-1-k}\right)\sum_{k=1}^{d=1} f'''_{d-1} - \frac{\kappa}{A_2}\left(\sum_{k=1}^{d=1} g'_{d-1-k}g'_j + \sum_{k=1}^{d=1} g'_{d-1-k}g''_k - 1\right) + \lambda^2 \\ & -A_1\left(\sum_{k=1}^{d=1} f''_{d-1-k}f_k - \sum_{k=1}^{d=1} f'_{d-1-k}f'_k + \ \alpha_1\left(\sum_{k=1}^{d=1} f'_{d-1-k} + \frac{\eta}{2}\sum_{k=1}^{d=1} f''_{d-1-k}\right)\right) + Gr\left(\theta_{d-1}+N\phi_d\right) \end{aligned}$$

$$\begin{aligned} R_d^g(\eta) \ = & \ \sum_{k=1}^{d=1} g''_{d-1-k} + \frac{A_5}{Pm}\left(\sum_{k=1}^{d=1} f_{d-}g''_{d-1-k} - \sum_{k=1}^{d=1} g_{d-}f''_{d-1-k}\right) - \frac{\alpha_1}{2}\left(\sum_{k=1}^{d=1} g\prime_d + \eta\sum_{k=1}^{d=1} g''_{d-1-k}\right) \\ R_d^\theta = & \left(A_4-\frac{4R_d}{3}\right)\sum_{k=1}^{d=1}\theta''_{d-1-k} + PrEc\left(1+\frac{1}{\gamma}\right)\sum_{k=1}^{d=1}\theta''_{d-1-k}\theta''_k - A_3\,\mathrm{Pr}\left(\alpha_1\frac{\eta}{2} - \sum_{k=1}^{d=1} f_k\right)\sum_{k=1}^{d=1}\theta'_k \\ & +A_4\alpha_0\sum_{k=1}^{d=1} g''_{d-1-k}g''_k + Du\sum_{k=1}^{d=1}\phi''_{d-1-k}\phi''_k + A_4\left(A^*\sum_{k=1}^{d=1} f'_{d-1-k} + B^*\theta_d\right) \end{aligned} \tag{3.37}$$

$$\begin{aligned} R_d^\phi = & \sum_{k=1}^{d=1}\phi''_{d-1-k}\phi''_k + Sr\sum_{k=1}^{d=1}\theta''_{d-1-k}\theta''_k - \beta\sum_{k-1}^{d-1}\left(\phi_d\sum_{k=1}^{d=1}\theta'_{d-1-k}\right) \\ & -\alpha_1\left(\frac{\eta}{2} - \sum_{k=1}^{d=1} f_k\right)\sum_{k=1}^{d=1}\phi'_{d-1-k} + \delta_1\phi(\eta)^n \end{aligned}$$

where

$$\chi \ = \ 0 \text{ when } d \ \leq \ 1$$

and

$$\chi \ = \ 1 \text{ when } d \ > \ 1$$

Hence, the general solutions are:

$$\begin{aligned} f_d(\eta) = & \ f_d(\eta)' \ + \ c_1 \ + \ c_2\eta \ + \ c_3\eta^2 \ + \ c_4\eta^3 \\ g_d(\eta) = & \ g_d(\eta)' \ + \ c_5 \ + \ c_6e^{\eta} \ + \ c_7e^{-\eta} \\ \theta_d(\eta) = & \ \theta_d(\eta)' \ + \ c_8e^{\eta} \ + \ c_9e^{-\eta} \end{aligned} \tag{3.38}$$

Here, $f_d(\eta)'$,$g_d(\eta)'$ and $\theta_d(\eta)'$ are the particular solution, while $c's$ are constants which were determined by the boundary conditions.
Lastly, the equations are coded and executed in a symbolic system Maple 2021 package.
The solution for the non-magnetic case is chosen as an initial guess and the iterations using Euler scheme are continued till convergence within prescribed accuracy is achieved, with the corrections incorporated in subsequent iterative steps until convergence, which is used to obtain the values of our initial guesses. Finally, the resulting guesses together with the system was solved using generalized Thomas' algorithm. The system of equations has to be solved in the infinite domain $0 < \infty < \eta_\infty$. A finite domain in the η-direction can be used instead with η chosen large enough to

ensure that the solutions are not affected by imposing the asymptotic conditions at a finite distance. Grid-independence studies show that the computational domain $0 < \infty < \eta_\infty$ can be divided into intervals each of uniform step size which equals 0.02. This reduces the number of points between $0 < \infty < \eta_\infty$ without sacrificing accuracy. The value $\eta_\infty = 5$ was found to be adequate for all the ranges of parameters studied here.

Table 3.1: Computed Initial Conditions at the wall

Parameters	$f'(\eta)$	$g'(0)$	$\theta(0)$	$\phi(0)$	Parameters	$f'(\eta)$	$g'(0)$	$\theta(0)$	$\phi(0)$
$\alpha_1 = 0.01$	0.90	1.27	0.36	1.02	$\Omega = 0.4$	0.90	1.24	0.36	1.02
$\alpha_1 = 0.05$	0.90	1.24	0.36	1.02	$\Omega = 0.8$	0.90	1.22	0.36	1.02
$\alpha_1 = 0.10$	0.90	1.19	0.36	1.02	$\Omega = 1.4$	0.90	1.18	0.36	1.02
$\alpha_1 = 0.20$	0.89	1.09	0.37	1.02	$\Omega = 2.4$	0.90	1.14	0.35	1.02
$Le = 0.5$	0.90	1.28	0.25	1.22	$\lambda = 0.0$	0.88	1.37	0.40	1.01
$Le = 0.$	0.90	1.25	0.31	1.11	$\lambda = 0.2$	0.90	1.23	0.35	1.02
$Le = 0.$	0.90	1.24	0.35	1.02	$\lambda = 0.4$	0.92	1.15	0.31	1.02
$Le = 0.$	0.90	1.23	0.43	0.85	$\lambda = 1.2$	1.07	1.01	0.28	1.02
$Sr = 0.0$	0.90	1.23	0.45	0.82	$\kappa_1 = 0.0$	0.90	1.24	0.35	1.02
$Sr = 0.2$	0.90	1.23	0.40	0.91	$\kappa_1 = 1.0$	0.89	1.22	0.36	1.02
$Sr = 04$	0.90	1.23	0.35	1.02	$\kappa_1 = 3.0$	0.87	1.20	0.37	1.02
$Sr = 0.5$	0.90	1.23	0.32	1.08	$\kappa_1 = 6.0$	0.86	1.17	0.39	1.01
$\beta = -0.5$	0.90	1.23	0.35	1.02	$N = 0.1$	0.89	1.22	0.35	1.02
$\beta = -0.1$	0.90	1.23	0.38	0.96	$N = 0.6$	0.90	1.24	0.35	1.02
$\beta = 0.1$	0.90	1.23	0.40	0.92	$N = 1.6$	0.91	1.26	0.34	1.02
$\beta = 0.5$	0.90	1.23	0.42	0.88	$N = 3.2$	0.93	1.30	0.33	1.02
$Rd = 0.00$	0.90	1.23	0.38	1.01	$Gr = 0.0$	0.89	1.22	0.36	1.02
$Rd = 0.05$	0.90	1.23	0.37	1.02	$Gr = 0.5$	0.90	1.24	0.35	1.02
$Rd = 0.10$	0.90	1.23	0.36	1.02	$Gr = 1.0$	0.91	1.25	0.34	1.02
$Rd = 0.25$	0.90	1.23	0.32	1.03	$Gr = 2.0$	0.93	1.29	0.34	1.02
$n = 0$	0.90	1.27	0.32	1.07	$V = 0.0.$	1.00	1.26	0.38	1.01
$n = 1$	0.90	1.23	0.36	1.02	$V = 0.0.2$	0.82	1.21	0.33	1.03
$n = 2$	0.90	1.23	0.36	1.01	$V = 0.0.4$	0.71	1.17	0.31	1.03
$n = 3$	0.90	1.23	0.36	1.01	$V = 0.8$	0.59	1.14	0.29	1.04
$Ec = 0.0$	0.90	1.23	0.26	1.04	$S = 0.0$	0.93	2.87	0.91	0.97
$Ec = 0.5$	0.90	1.23	0.35	1.02	$S = 0.4$	0.93	1.87	0.60	1.03
$Ec = 1.0$	0.90	1.23	0.44	1.00	$S = 0.8$	0.92	1.50	0.47	1.04
$Ec = 1.5$	0.90	1.24	0.54	0.97	$S = 1.2$	0.91	1.32	0.39	1.03
$\alpha_0 = 0.0$	0.90	1.23	0.34	1.02	$Bi = -0.5$	0.90	1.23	0.18	0.81
$\alpha_0 = 0.1$	0.90	1.23	0.35	1.02	$Bi = -0.1$	0.89	1.23	0.02	0.57
$\alpha_0 = 0.2$	0.90	1.23	0.36	1.02	$Bi = 0.1$	0.90	1.23	0.35	1.02
$\alpha_0 = 0.5$	0.90	1.24	0.39	1.01	$Bi = 0.5$	0.90	1.23	0.24	0.89
$Du = 0.0$	0.89	1.21	0.37	1.01	$r = 0.1$	0.91	1.26	0.61	3.72
$Du = 1.0$	0.89	1.21	0.36	1.01	$r = 0.5$	0.90	1.24	0.42	1.69
$Du = 2.0$	0.90	1.21	0.35	1.02	$r = 1.0$	0.90	1.23	0.35	1.02
$Du = 2.5$	0.90	1.21	0.35	1.02	$r = 1.6$	0.90	1.23	0.32	0.69
$\delta = -0.6$	0.90	1.23	0.37	0.98	$\varphi = 0.0$	0.88	1.17	0.30	1.03
$\delta = -0.2$	0.90	1.23	0.36	1.00	$\varphi = 0.2$	0.95	1.53	0.57	0.96
$\delta = 0.2$	0.90	1.23	0.35	1.02	$\varphi = 0.6$	0.99	1.85	0.75	0.91
$\delta = 0.6$	0.90	1.23	0.34	1.04	$\varphi = 0.8$	1.03	2.39	0.96	0.85

The Graphical Representation and Analysis of Results,

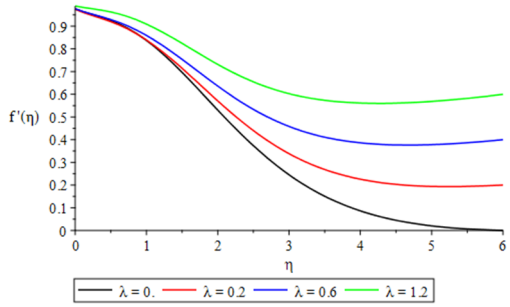

Figure 3.2: Graph of velocity for various values stretching parameter λ

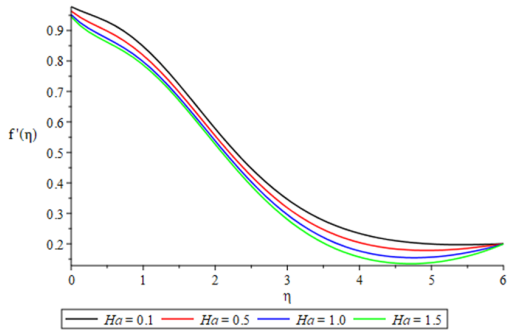

Figure 3.3: Graph of velocity for various values Hartmann Number Ha

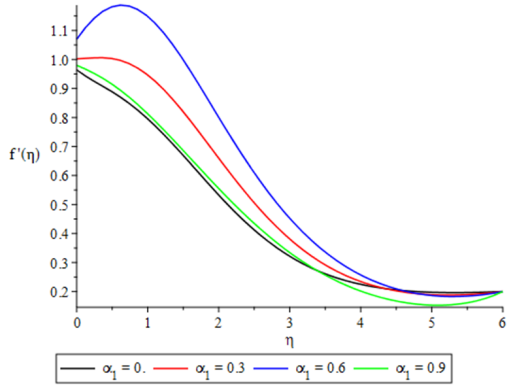

Figure 3.4: Graph of velocity for various values unsteadiness parameter α_1

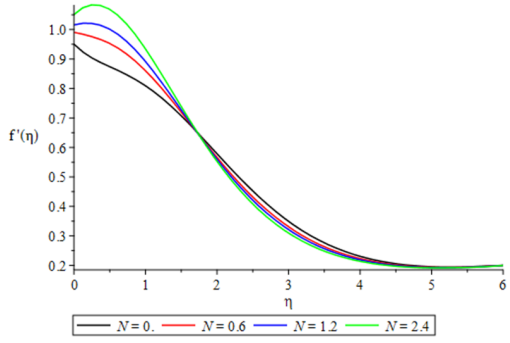

Figure 3.5: Graph of velocity for various values Buoyancy parameters N

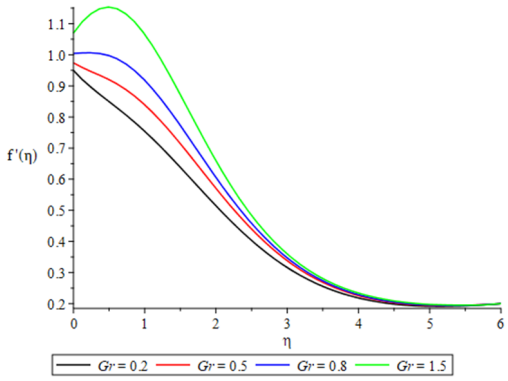

Figure 3.6: Graph of velocity for various values Grashof number Gr

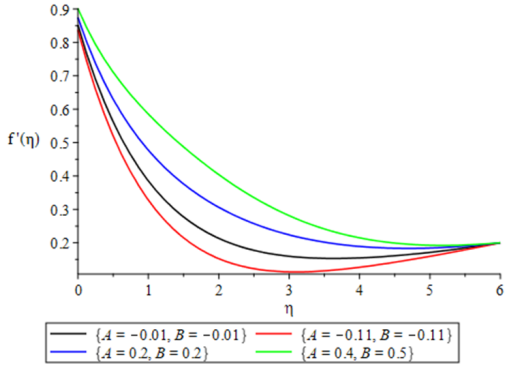

Figure 3.7: Graph of velocity for various values space heat generation/absorption parameter A, B

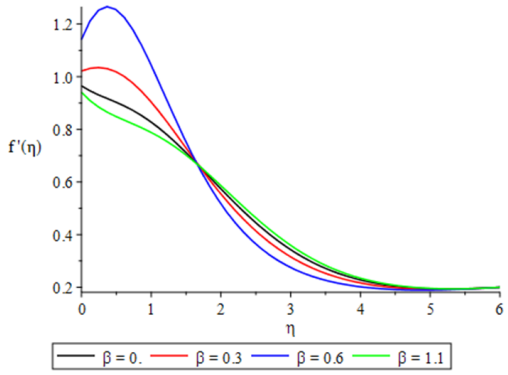

Figure 3.8: Shows the effect of thermophoretic force β on velocity distribution.

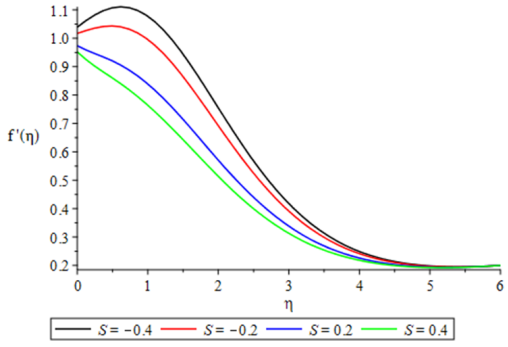

Figure 3.9: Graph of velocity for various injection/suction parameter S

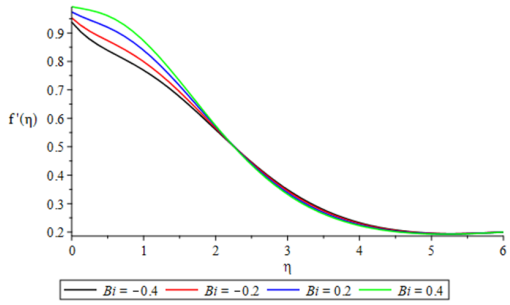

Figure 3.10: Graph of velocity for various values stretching parameter B_i

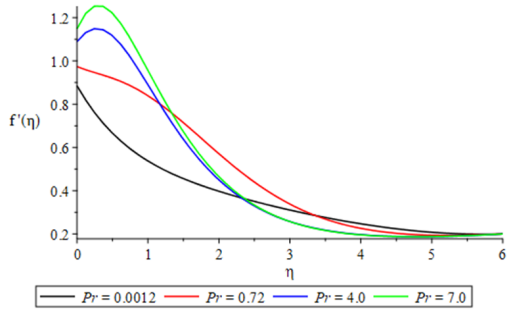

Figure 3.11: Graph of velocity for various values stretching parameter Pr

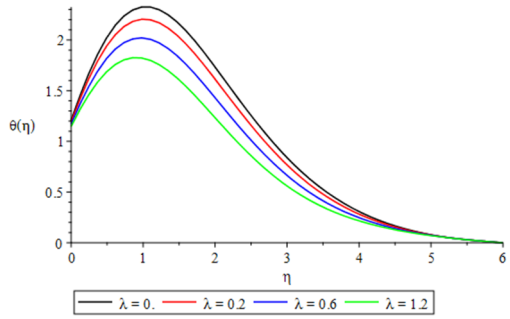

Figure 3.12: Graph of temperature for various values stretching parameter λ

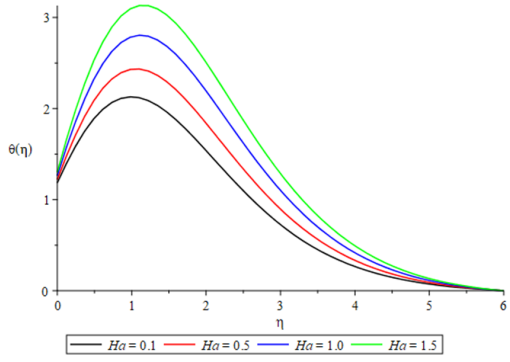

Figure 3.13: Graph of temperature for various values stretching parameter Ha

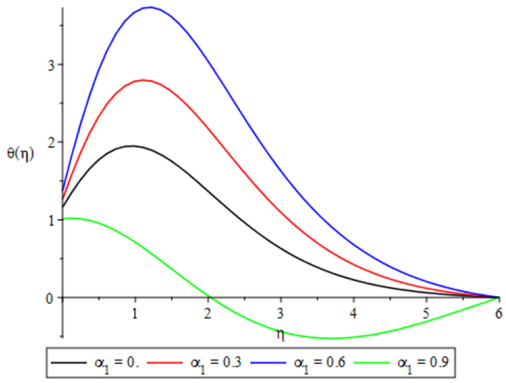

Figure 3.14: Graph of temperature for various values stretching parameter α_1

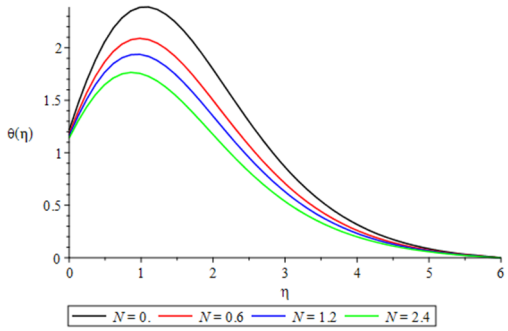

Figure 3.15: Graph of temperature for various values stretching parameter N

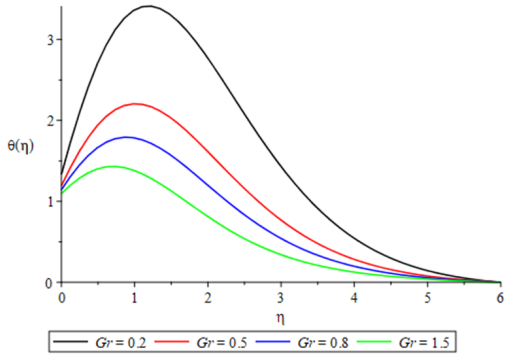

Figure 3.16: Graph of temperature for various values stretching parameter Gr

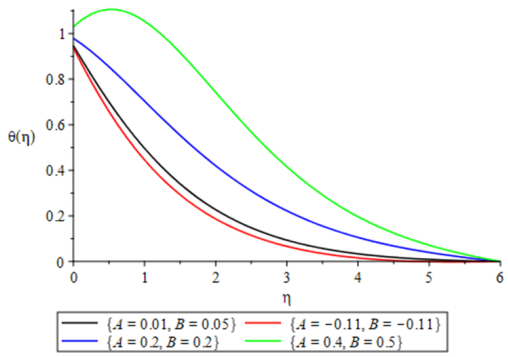

Figure 3.17: Graph of temperature for various values stretching parameter A, B

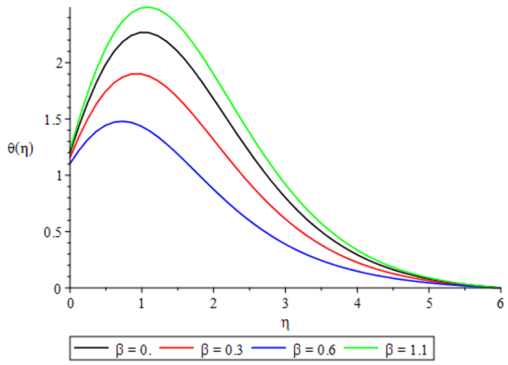

Figure 3.18: Graph of temperature for various values stretching parameter β

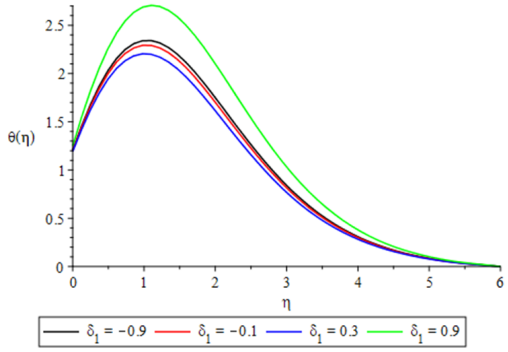

Figure 3.19: Graph of temperature for various values stretching parameter δ_1

4. Conclusion

The comprehensive analysis of magnetohydrodynamics (MHD), nanoparticles, slip conditions, and non-uniform heating in fluid flow over a nonlinear stretching wedge provides valuable insights into their intricate interplay. Through numerical simulations and theoretical investigations, this research elucidates complex fluid dynamics and thermal behavior, paving the way for advancements in engineering applications. The significant influence of MHD and nanoparticles on flow patterns, temperature distributions, and heat transfer rates is underscored, offering opportunities for tailored control and optimization of processes. Leveraging MHD techniques and nanoparticle additives holds promise for enhancing heat transfer and fluid transport in various applications, including heat exchangers, microfluidic devices, and thermal management systems. Insights gained have implications for biomedical engineering, aerospace propulsion, and energy conversion, addressing critical challenges and advancing technological frontiers. The analysis of slip conditions and non-uniform heating profiles highlights their role in influencing flow behavior and thermal gradients, essential for optimizing design in microfluidics, lubrication, and surface coating. Overall, this research contributes to understanding complex fluid dynamics and thermal behavior, informing the development of innovative engineering solutions across diverse applications

Financial Support

No financial support is obtained in the course of this research

Acknowledgement

Authors acknowledged the tremendous efforts of all academic staff of the Department of mathematics and Statistics Osun State College of Technology, Esa-Oke and Mathematical Sciences, Osun State University Osogbo.

Declaration

The authors of the paper declared that there are no conflicts of interest.

Authorship Contribution Statement

Victor A. Akinrinmade: Methodology, Data preparation, reviewing, and editing
Mutairu K. Kolawole: Data preparation, analysis, reviewing and supervision, Data preparation, reviewing

References

[1] M. Abramowitz and I. A. Stegun, *Handbook of mathematical functions*. Dover Publications, 1965. View online.
[2] R. Al-Hussainy, H. Ramey Jr, and P. Crawford, "The flow of real gases through porous media," *journal of Petroleum Technology*, vol. 18, no. 05, pp. 624–636, 1966. View online.
[3] D. Dietz, "Determination of average reservoir pressure from build-up surveys," *Journal of Petroleum Technology*, vol. 17, no. 08, pp. 955–959, 1965. View online.
[4] P. Eykhoff, *System identification*. Wiley London, 1974. View online.
[5] W. J. Lee and S. A. Holditch, "Application of pseudotime to buildup test analysis of low-permeability gas wells with long-duration wellbore storage distortion," *Journal of Petroleum Technology*, vol. 34, no. 12, pp. 2877–2887, 1982. View online.
[6] J. Lee, J. B. Rollins, and J. P. Spivey, *Pressure transient testing*. SPE, 2003. View online.
[7] J. C. Martin, "Simplified equations of flow in gas drive reservoirs and the theoretical foundation of multiphase pressure buildup analyses," *Transactions of the AIME*, vol. 216, no. 01, pp. 321–323, 1959. View online.
[8] J. Naar and R. Wygal, "Three-phase imbibition relative permeability," *Society of Petroleum Engineers Journal*, vol. 1, no. 04, pp. 254–258, 1961. View online.
[9] H. Stone, "Probability model for estimating three-phase relative permeability," *Journal of petroleum technology*, vol. 22, no. 02, pp. 214–218, 1970. View online.
[10] H. Stone, "Estimation of three-phase relative permeability and residual oil data," *Journal of Canadian Petroleum Technology*, vol. 12, no. 04, 1973. View online.
[11] G. P. Willhite, *Waterflooding*. Society of Petroleum Engineers, Richardson, TX, 1986. View online.
[12] J. H. Biagi, *Numerical simulation and optimization of carbon dioxide utilization and storage in enhanced gas recovery and enhanced geothermal systems*. Washington University in St Louis, 2014. View online.
[13] C. M. Oldenburg, "Carbon sequestration in natural gas reservoirs: enhanced gas recovery and natural gas storage," in *Proceedings TOUGH Symposium '03*, 2003. View online.
[14] X. Feng, B. Zhong, Y. Liu, Y. Chu, and L. Chen, "Multi-factor coupling analysis of optimized gas-well production allocation," *Nat Gas Ind*, vol. 32, no. 1, pp. 53–58, 2012. View online.
[15] F. Forouzanfar and A. Reynolds, "Well-placement optimization using a derivative-free method," *Journal of Petroleum Science and Engineering*, vol. 109, pp. 96–116, 2013. View online.

[16] F. Forouzanfar, A. C. Reynolds, and G. Li, "Optimization of the well locations and completions for vertical and horizontal wells using a derivative-free optimization algorithm," *Journal of Petroleum Science and Engineering*, vol. 86, pp. 272–288, 2012. View online.
[17] D. I. Gerogiorgis, M. Georgiadis, G. Bowen, C. Pantelides, and E. Pistikopoulos, "Dynamic oil and gas production optimization via explicit reservoir simulation," vol. 21, pp. 179–184, 2006. View online.
[18] Z. Huang, R. Wang, and J. Du, "Effect analysis of withdraw gas recovery in xujiahe 2 gas reservoir of zhongba gas reservoir," *Drill Prod Technol*, vol. 35, no. 6, pp. 51–54, 2012. View online.
[19] Y. I. Kalugin, V. Yakovlev, and A. Y. Kalugin, "Mathematical modeling and optimization of gas-condensate field development," *Journal of Natural Gas Science and Engineering*, vol. 27, pp. 1195–1204, 2015. View online.
[20] D. Krishnamoorthy, B. Foss, and S. Skogestad, "Real-time optimization under uncertainty applied to a gas lifted well network," *Processes*, vol. 4, no. 4, p. 52, 2016. View online.
[21] X. Liao, Q. Meng, Y. Yang, and W. Chen, "Using high voltage sub-transmission technology to increase gas recovery in xin-chang gas reservoir," *Nat Gas Oil*, vol. 21, no. 2, pp. 18–26, 2003. View online.
[22] G. Ping, J. Shasha, and P. Caizhen, "Technologies and countermeasures for gas recovery enhancement," *Natural Gas Industry B*, vol. 1, no. 1, pp. 96–102, 2014. View online.
[23] S. Ren, "Optimization design of gas pool fracturing in suining group of luodai gas field," *Drilling and Production Technology*, vol. 30, no. 2, p. 65, 2007. View online.
[24] M. Samuelson, T. Akinwande, R. Connell, R. Grossman, and B. Strickland, "Optimizing horizontal completions in the cleveland tight gas sand," in *SPE Unconventional Resources Conference/Gas Technology Symposium*, pp. SPE–113487, SPE, 2008. View online.
[25] L. Xiaogang, X. He, Z. Yang, and L. Chun, "Difficulties and countermeasures of hydraulic fracturing of the inefficient sandstone gas reservoir in western sichuan," *Drill Prod Technol*, vol. 33, no. 6, pp. 49–51, 2010. View online.
[26] Q. P. Zheng, S. Rebennack, N. A. Iliadis, and P. M. Pardalos, "Optimization models in the natural gas industry," *Handbook of Power Systems I*, pp. 121–148, 2010. View online.

Citation IEEE Format:
V. A. Akinrinmade and M. K. Kolawole. *"Coupled Effects of Magnetohydrodynamics and Nanoparticles on Nonlinear Stretching Wedge Flow with Multiple Slips and Non-Uniform Heating"*, *Jurnal Diferensial*, vol. 6(2), pp. 108-123,2024.